minerals

MDPI

Article

Solid Carriers of Potentially Toxic Elements and Their Fate in Stream Sediments in the Area Affected by Iron Ore Mining and Processing

Saša Kos [1,*], Nina Zupančič [2,3], Mateja Gosar [1] and Miloš Miler [1]

[1] Geological Survey of Slovenia, Dimičeva ulica 14, SI-1000 Ljubljana, Slovenia
[2] Department of Geology, Faculty of Natural Sciences and Engineering, University of Ljubljana, Aškerčeva cesta 12, SI-1000 Ljubljana, Slovenia
[3] Ivan Rakovec Institute of Palaeontology, Research Centre of the Slovenian Academy of Sciences and Arts, Novi trg 2, SI-1000 Ljubljana, Slovenia
* Correspondence: sasa.kos@geo-zs.si

Abstract: The potential environmental impact of historical mining and ore processing on stream sediments and water was studied in a small siderite iron ore deposit with diverse sulfide mineral paragenesis. The main aim was to characterize solid carriers of potentially toxic elements (PTEs) in stream sediments and mine waste, to understand their fate in fluvial systems. General mineralogy (X-ray powder diffraction) and individual solid PTE carriers (scanning electron microscopy/energy dispersive spectroscopy) were correlated with the geochemical composition of stream sediments, mine waste, and stream waters (inductively coupled plasma mass spectrometry). Primary solid PTE carriers were pyrite, chalcopyrite, sphalerite, Hg-bearing sphalerite, galena, and siderite. Slightly alkaline and oxidizing conditions in stream water promoted the transformation of primary phases into secondary PTE carriers. Fe(Mn)-oxide/oxyhydroxides were major sinks for Pb, Zn, and As. Compared to background levels, Co (14.6 ± 2.1 mg/kg), Cu (30 ± 2.9 mg/kg), Ni (32.1 ± 2.9 mg/kg), Pb (64.5 ± 16.4 mg/kg), Zn (175.3 ± 22.5 mg/kg), As (81.1 ± 63.7 mg/kg), and Hg (2 ± 0.8 mg/kg) were elevated in mining area. Mine waste contained similar PTE carriers as stream sediments, but much higher PTE contents. Prevailingly low PTE concentrations in streams, with the exception of As (1.97 ± 2.4 µg/L) and Zn (4.5 ± 5.7 µg/L), indicate the stability of PTE carriers. Environmental effects were not significant, and additional monitoring is recommended.

Keywords: environmental mineralogy; environmental geochemistry; potentially toxic elements; stream sediments; solid phases; iron ore deposit; SEM/EDS

Citation: Kos, S.; Zupančič, N.; Gosar, M.; Miler, M. Solid Carriers of Potentially Toxic Elements and Their Fate in Stream Sediments in the Area Affected by Iron Ore Mining and Processing. *Minerals* **2022**, *12*, 1424. https://doi.org/10.3390/min12111424

Academic Editor: Alexandra Courtin-Nomade

Received: 30 September 2022
Accepted: 8 November 2022
Published: 10 November 2022

1. Introduction

Mineralized rocks are a natural source of potentially toxic elements (PTEs). PTEs occur as constituents of primary ore minerals, resistant secondary minerals, and precipitates of various types [1]. Potential contaminants can spread in the environment through weathering, erosion, and transport by water and wind from naturally enriched or contaminated sites. The exploitation of metal ore deposits leads to additional anthropogenic dispersal and an increase in PTEs in the environment. Stream sediments are an excellent medium for the study of solid PTE carriers. Under favorable conditions, solid phases play an important role in the storage and remobilization of PTEs in fluvial systems [2,3]. Because of their ability to accumulate PTEs, stream sediments can reflect water quality and record the effects of anthropogenic emissions [4]. The interactions of PTEs with water and stream sediments are strongly influenced by the physico-chemical characteristics of the water, including pH, redox potential, dissolved oxygen, and ionic species, and in the case of stream sediments, by the mineralogy and properties of the individual solid phases [5,6]. Certain PTEs such as

As, Cd, Hg, Pb, etc., are toxic even in trace amounts, so knowledge of their solid carriers and behavior in the environment is very important [7].

Metal mining and metallurgical processing have a long history in Slovenia, leaving behind numerous mines and ore-processing waste dumps that still pose a potential threat to the environment [8,9]. So far, only the environmental impacts of the largest metal mines such as Mežica (Pb, Zn), Idrija and Podljubelj (Hg), and Litija (Pb, Hg, Zn, Fe, Ba) have been studied [10–20]. The Sava Caves iron ore deposit near Jesenice in northwestern (NW) Slovenia was mined for 500 years until the start of the 20th century [21]. Iron ore was roasted in the Sava Caves until the 17th century. In addition to iron ore, lead and zinc sulfides were occasionally roasted [22,23]. The sulfide-bearing rock, which may contain a high content of PTEs (As, Cd, Co, Hg, Ni, Sb, Sn, and Zn) [24,25] was probably disposed of as overburden near the mine shafts. The impacts of mining, ore processing, and mine waste disposal on the environment in the Sava Caves have not yet been studied, and the behavior of the solid PTE carriers has not yet been determined.

The main objectives of this study were (i) to identify primary and secondary solid PTE carriers in stream sediments and mine waste, (ii) to determine the contents and distribution of PTEs in stream sediments, mine waste, and waters, (iii) to understand the stability of primary and secondary solid PTE carriers in the fluvial system, and (iv) to evaluate the impacts of geogenic and anthropogenic processes on the environment of the Sava Caves iron ore deposit.

2. Materials and Methods

2.1. Study Area Description

The study area of the Sava Caves iron ore deposit (46.47° N, 14.07° E) is located in northwestern (NW) Slovenia in the Western Karavanke Mountains, about 5 km from the industrial town of Jesenice (Figure 1). Situated between an altitude of 900 and 1300 m, the area is characterized by mountainous terrain and mixed forests, surrounding a narrow valley of the Črni potok creek. The mean annual rainfall in the area is 1790 mm with a mean annual temperature of 6.7 °C [26]. The Črni potok is a short tributary that drains the area of the Sava Caves and eventually joins the Sava River in the Upper Sava Valley [27]. The main mining facilities and roasting plants in the Sava Caves were located along the Črni potok stream at about 1100 m above sea level.

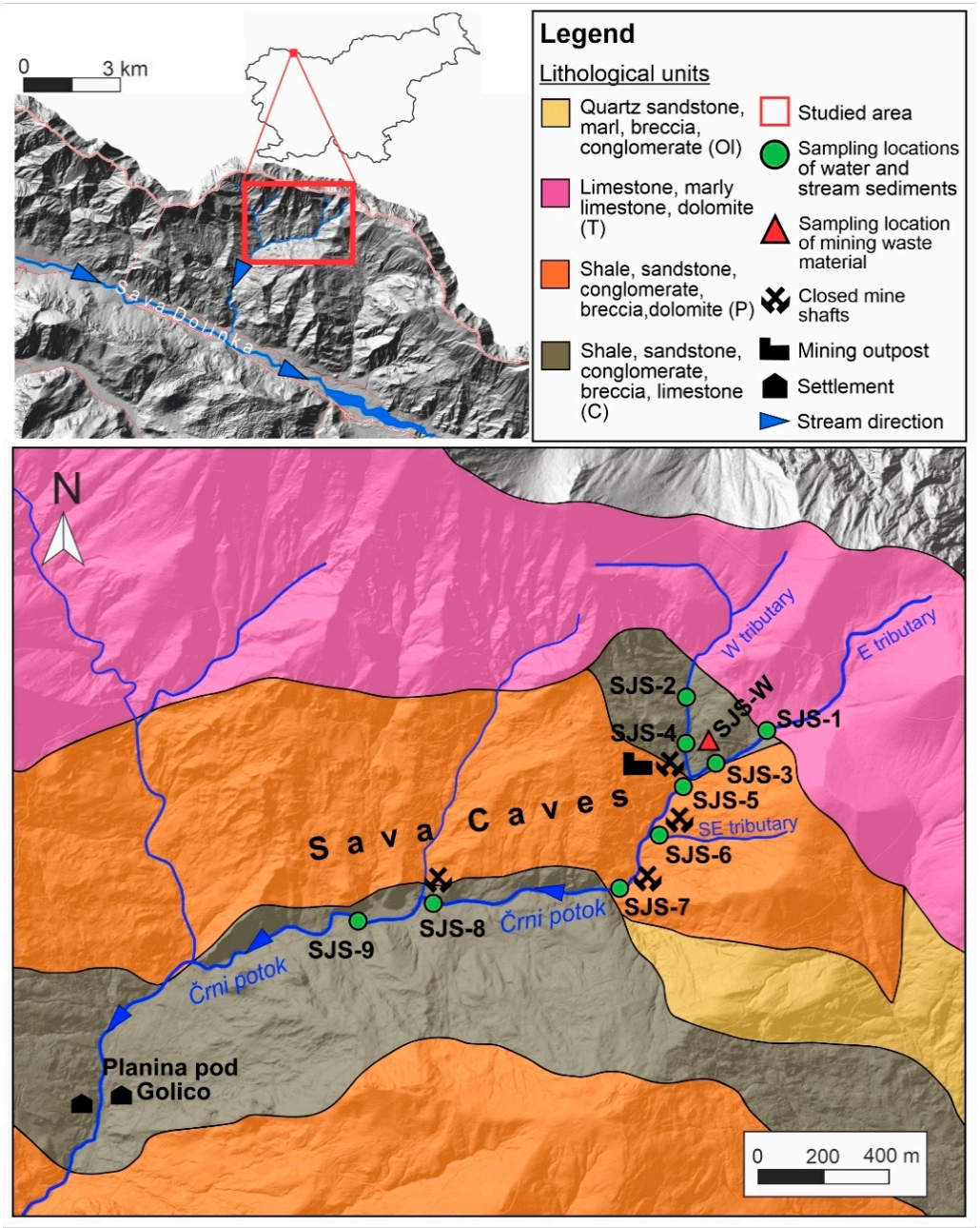

Figure 1. A topographic map with generalized lithology of Oligocene (Ol), Triassic (T), Permian (P), and Carboniferous (C) rocks [28]. Sampling locations of samples SJS-W (mine waste) and SJS-1 to SJS-9 (stream sediment), closed mine shafts, mining outposts, and mine waste in the area of the Sava Caves are presented on the map.

2.2. Geology of the Study Area

The Sava Caves are an upper Palaeozoic hydrothermal-metasomatic iron ore deposit formed under meso- and epithermal conditions [25,29,30]. Mineralization with the primary ore mineral siderite occurs as veins and lenses at the contact between Devonian and Carboniferous rocks [30], particularly in Upper Carboniferous limestones and, to a lesser extent, in Upper Carboniferous sandstones and shales. Siderite is accompanied by a variety of sulfide minerals consisting primarily of galena and sphalerite, but also pyrite, chalcopyrite, realgar, and orpiment occur in the mineral paragenesis. The secondary minerals anglesite, cerussite, smithsonite, azurite, and malachite were also determined [24,31]. According to Schroll [25], sphalerite may contain higher contents of Fe (5%) and Cd (0.5%) and minor

contents of Co, Ga, Ge, Hg, In, Ni, Sn, and Sb (<500 mg/kg). Galena may contain Ag, Bi, and Sb [25]. The ore bodies were strongly deformed by intense tectonics; consequently, the mine shafts were scattered on the slope of Golica Mountain. In its upper part, the Črni potok catchment area is lithologically characterized by Triassic limestones and dolomites, while the lower part consists mainly of Upper Palaeozoic sandstones and siltstones (Figure 1).

2.3. Sample Collection and Preparation

A total of nine (9) samples (SJS-1 to SJS-9) were collected from the recent active stream sediment of the Črni potok stream and its main tributaries (western (W), eastern (E) and southeastern (SE); Figure 1) in November 2014. Two samples (SJS-1 and SJS-2) were collected upstream of the mining area to evaluate the geochemical background, and the remaining samples were collected downstream at locations where mining took place. A composite of at least 1 kg of active stream sediment was collected at each site and sampled at five sub-sites.

In the upper part of the area (Figure 1), above the former mining settlement, was a partially weathered mine waste heap consisting of a mixture of soil and gravel, most probably gangue, poor ore, and ore roasting waste. A composite sample (SJS-W) was collected from the upper 25 cm for comparison with the stream sediments.

Samples of stream sediments and mine waste material were oven dried for 14 days at 40 °C to avoid losses of Hg [32] and sieved through stainless steel sieves. The grain size fraction below 0.125 mm was prepared for chemical, mineralogical, and individual particle analyses. This grain size fraction was selected according to standardized preparation procedures for stream sediments [10,11,16,17,20]. A heavy mineral fraction with a density higher than 2.89 g/cm^3 was prepared from approximately 10 g of samples SJS-2, SJS-4, SJS-5, SJS-6, SJS-8, and SJS-W (<0.125 mm) using bromoform (ρ = 2.89 g/cm^3 at 25 °C). The heavy mineral fractions represent 1 to 2.5% of the stream sediment samples, while in the mine waste material the proportion of heavy minerals was less than 1%.

The water of the Črni potok creek was sampled at the same sampling locations as stream sediments only in June 2020. Samples were filtered with sterile polypropylene syringes through 0.45 µm sterile surfactant-free cellulose acetate filters and stored in rinsed 50 mL high-density polyethylene bottles at 5 °C until chemical analysis.

2.4. Mineralogical Characterization and Microanalytical Single Particle Analysis

The mineral composition of the stream sediment was determined by X-ray powder diffraction (XRD) analysis using a Phillips PW3710 X-ray powder diffractometer equipped with Cu Kα tube and secondary graphite monochromator operated at 40 kV and 20 mA. Samples were scanned from 2° to 70° 2θ, with step size 0.02° and a count time of 0.4 s/step. Oriented samples for clay mineral identification were prepared by ultrasonic dispersion, centrifugation, and the glass slide method. Diffraction patterns were interpreted using PANalytical X'Pert HighScore Plus 4.1 diffraction software and the PAN-ICSD 3.4 database. A semi-quantitative analysis was done by determining the background of each diffractogram. The relative volume fraction of each mineral was estimated for every sample by evaluation of several parameters, including total diffraction peak intensity, goodness of peak fits, and contribution to the overall fitting [33]. The relative mineral composition was determined for the crystalline phase only.

Morphological and semi-quantitative chemical identification of individual solid PTE carriers was performed on loose particle samples (<0.125 mm size fraction) and heavy-mineral fractions. Samples were mounted on double-sided carbon tape and carbon-coated for conductivity. The scanning electron microscopy coupled with energy dispersive spectrometer (SEM/EDS) analysis was performed in a high vacuum using a JEOL JSM 6490LV SEM coupled with an Oxford INCA PentaFETx3 Si(Li) EDS at an accelerating voltage of 20 kV (spot size 48 and 50; working distance 10 to 11 mm). The INCA Energy 350 EDS software was calibrated for quantification using pre-measured universal standards, following the fitted standards procedure [34], referenced to a cobalt (Co) optimization standard.

Correction of data from EDS was performed using the standard ZAF correction procedure included in the INCA Energy software [35]. Samples were analyzed in backscattered electron (BSE) mode, which allowed the relative distinction of elemental composition. The EDS elemental mapping of multiple fields-of-view was performed for each sample at a magnification of 100× and an acquisition time of 700 s to determine the spatial distribution of elements and estimate relative mineral and phase abundances. The PTE carriers were then characterized based on size, morphology, and chemical composition using EDS X-ray point analysis with 60 s of acquisition time. The possible mineral equivalents were evaluated based on the atomic proportions of the constituent elements and comparison with the atomic proportions of known stoichiometric minerals, using available mineral databases [36,37].

2.5. Chemical Analysis of Stream Sediments and Mine Waste Material

The contents of PTEs (As, Cd, Co, Cr, Cu, Fe, Hg, Mn, Mo, Ni, Pb, Sb, and Zn) in the stream sediment and mine waste samples were determined at Bureau Veritas Mineral Laboratories, Vancouver, British Columbia, Ancaster, ON, Canada, using inductively coupled plasma mass spectroscopy (ICP-MS) after digestion of 15 g samples with aqua regia (90 mL of HCl:HNO_3:H_2O in a 1:1:1 ratio heated in a water bath at 95 °C for 60 min) [38]. Accuracy of the analytical method was estimated by calculation of the relative systematic error (RSE) between the measured and recommended values of reference materials (STD DS10 and OREAS 45P) [39]. Relative systematic error based on STD DS10 for selected PTEs was in the range of 0.28 (Cu) to 22.1% (Sb) with a mean of 6.7%. Based on OREAS 45P, the RSE was in the range of 0.096 (Co) to 22.2% (Cd) with a mean of 9.7%. The precision was estimated from relative differences between duplicate measurements by calculating the relative percentage difference (%RPD). The mean RPD was 2.9% and the highest for Hg (9.96%). An entire chemical analysis data set along with quality control for stream sediments and mine waste was also provided as Supplementary Spreadsheet S1.

2.6. Chemical Analysis of Stream Water

Major (Al, Ca, K, Mg, Na, S, Si) and trace (As, Cd, Co, Cr, Cu, Hg, Mo, Ni, Pb, Sb, Zn) element chemistry of stream waters was determined using a combination of ICP-MS and inductively coupled plasma–optical emission spectrometry (ICP-OES) at Activation Laboratories Ltd., Ancaster, ON, Canada. Prior to analysis, samples were acidified in the laboratory with ultra-pure nitric acid to pH < 2 to dissolve potentially precipitated elements. The accuracy (RSE) of analytical methods for selected elements ranged from 0.5 (Mg) to 20.4% (Zn) with a mean of 7.1%, based on reference material IV STOCK-1643 [40]. The RPD for measured duplicates was in the range of 0–16.2% (Pb) with a mean of 3.5%. An entire chemical analysis data set and quality control for stream waters was also provided as Supplementary Spreadsheet S2.

2.7. Physico-Chemical Properties of Stream Water

Measurements of temperature (T), pH, redox potential (Eh), conductivity (EC), and dissolved oxygen (DO) were performed on-site at the same time as water sampling, to determine physico-chemical parameters of the stream water using the Thermo Scientific Multimeter Orion Star A329. The pH electrode has an accuracy of ±0.03 and a precision of ±0.01 pH. The epoxy refillable redox potential electrode has an accuracy of ±60 mV, while the DO electrode with a built-in temperature sensor has an accuracy of ±0.2 mg/L and 0.3 °C, respectively.

3. Results and Discussion

3.1. Mineralogical Characteristics of Stream Sediments and Mine Waste Material

The main minerals found in stream sediments (size fraction < 0.125 mm) determined by XRD were quartz (23–51%), dolomite (13–51%), muscovite/illite (10–24%), kaolinite (2–13%), and feldspars (5–15%) (Figure 2). Calcite and iron minerals–goethite, hematite,

and pyrite were present in trace amounts. The background lithology (Figure 1) contributed a large amount of carbonate material to the stream channel. Dolomite and calcite content steadily decreases downstream. Quartz and aluminosilicate minerals contents increase, as the channel erodes through the siliciclastic bedrock. The SE tributary contributes a large amount of quartz (51%) and aluminosilicate minerals (43%) to the main stream channel. Higher carbonate material content (22%) was observed again in sample SJS-8, indicating re-contact of the stream with carbonate material. The mine waste sample (SJS-W) was dominated by quartz (45%), followed by the clay minerals kaolinite (23%), muscovite/illite (20%), and minor amounts of feldspars (7%) and calcite (5%).

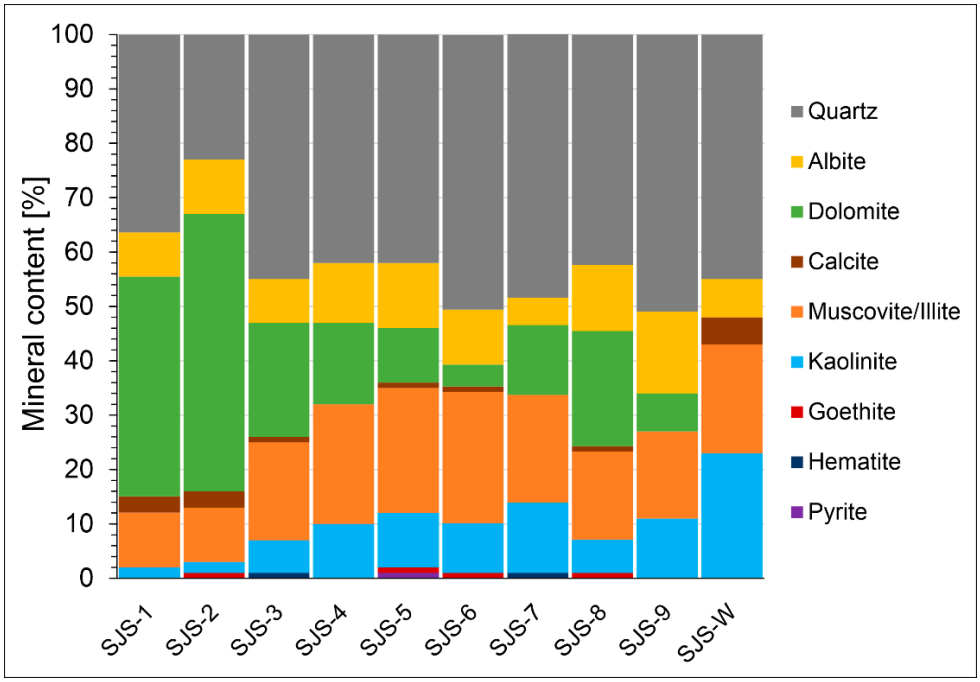

Figure 2. Semi-quantitative distribution of main minerals in stream sediments determined by XRD analysis and expressed in %. Mineral distribution in mine waste (SJS-W) is shown for comparison.

The general mineral composition was confirmed by the SEM/EDS elemental mapping. Aluminosilicates and quartz (50%–60%) predominate over Mg/Ca carbonates (20%–30%). A large proportion of aluminosilicates contains K and Fe. Mapping revealed a small proportion of solid Fe and Mn phases (5%–10%), including crystalline or amorphous sulfide, carbonate, oxide, or oxyhydroxide minerals.

3.2. Solid PTE Carriers and Their Characteristics

The general composition of solid PTE carriers identified with SEM/EDS in stream sediments and mine waste material is presented in Table 1. PTEs are mainly bound to primary and secondary ore mineral phases, while the leached PTEs were mainly precipitated and attenuated by Fe and Mn solid phases. All identified solid PTE carriers were assigned to three groups according to the main constituent element. Solid Fe carriers, Zn carriers, and Pb carriers were described in the following sections according to their relative abundance in stream sediment and mine waste.

Table 1. Solid PTE carriers identified with SEM/EDS in stream sediments and mine waste material with common minor constituent elements, their relative abundance, and possible mineral equivalents. (Abundance: ***** very high, **** high, *** medium, ** low, * scarce).

Phase	Minor Constituent Elements	Relative Abundance	Mineral Equivalent
Fe-S		*****	Pyrite (FeS_2)
Fe-S-O	Ag, As, Cu, Pb	**	Szomolnokite ($FeSO_4 \cdot H_2O$)
Cu-Fe-S		*	Chalcopyrite ($CuFeS_2$)
Fe(Mn)-O	Pb, Zn	*****	Siderite ($FeCO_3$)/ferrihydrite ($Fe^{3+}{}_{10}O_{14}(OH)_2$/goethite ($\alpha$-$Fe^{3+}O(OH)$)/ lepidocrocite ($\gamma$-$Fe^{3+}O(OH)$)/hematite ($\alpha$-$Fe_2O_3$)/magnetite ($Fe^{2+}Fe_2{}^{3+}O_4$)
Fe-O	As, Cr, Pb, Ni, Zn	****	Ferrihydrite/goethite/lepidocrocite/ hematite/magnetite
Fe-Pb-Mn-O		*	Plumboferrite ($Pb_2(Fe^{3+}, Mn^{2+}, Mg)_{11}O_{19}$)
Fe-Mn-Mg-O	Pb	*	Jacobsite ($Mn^{2+}Fe^{3+}{}_2O_4$)
Zn-S	Cd, Fe, Hg	****	Sphalerite (ZnS)
Zn-(C)-O		*	Zincite (ZnO)/hydrozincite ($Zn_5(CO_3)_2(OH)_6$)/smithsonite ($ZnCO_3$)
Pb-S		***	Galena (PbS)
Pb-S-O		***	Anglesite ($PbSO_4$)
Pb-(C)-O	As, Cu	***	Cerussite ($PbCO_3$)/litharge (PbO_2)/massicot (PbO_2)
Pb-Si-O		*	Alamosite ($PbSiO_3$)

3.2.1. Solid Fe Carriers

Solid Fe carriers identified in both stream sediments and mine waste were pyrite, chalcopyrite, Fe-S-O solid phase, Fe(Mn)-oxide/oxyhydroxide, and Fe-oxide/oxyhydroxide solid phases.

Pyrite was a very common ore mineral in the stream sediment and mine waste. Pyrite formed cubic, mostly octahedral, euhedral single crystals (Figure 3a) or crystal clusters, but it also occurred in framboidal forms (Figure 3c). Chalcopyrite was found in the stream sediments as anhedral, subangular, massive particles (Figure 3b), although it was less abundant. The surface of most pyrite and chalcopyrite grains in stream sediments was corroded, with visible corrosion pits, or abraded by transport. Due to the rapid oxidative weathering of pyrite under surface conditions, Fe-S-O or Fe-O solid phases were detected on the surfaces of pyrite. These phases may also be Fe-oxyhydroxy sulfates and Fe-oxyhydroxides, which are common in aqueous environments [41]. The oxidized pyrites generally exhibited shrinkage cracks on the surface (Figure 3d). Mineralogical studies by Huggins et al. [42] revealed that pyrite first transforms to szomolnokite by oxidation, which gradually oxidizes to lepidocrocite and eventually ages to goethite. Although the pyrites did not exhibit other PTEs, the oxidation products on pyrites found in the stream sediments showed an affinity for Ag, As (Figure 3d), Cu, and Pb. The presence of these elements is related to other ore minerals, with which pyrite co-occurs in the ore zone.

The Fe(Mn)-oxide/oxyhydroxide and Fe-oxide/oxyhydroxide phases were found mainly as secondary precipitates occurring as coatings of very finely crystalline particles over various minerals (Figure 4a,b). Manganese (Mn) commonly substitutes for Fe [43]. The conditions for their formation were suitable in both stream sediments and mine waste. The coatings and agglomerate-like particles, which contain minor Mn, can be described as goethite or lepidocrocite, according to Rahimi et al. [44]. Both solid phases are initially formed as ferrihydrite, a poorly ordered metastable phase of fine particle size, which can eventually transform into goethite/lepidocrocite and/or hematite and magnetite under various physico-chemical conditions [45]. Large and massive, anhedral, angular to subangular particles of Fe(Mn)-O with minor Zn content, most probably siderite (Figure 4c), were found in stream sediment and mine waste. Their massive morphology is consistent

with primary mineralization. A subangular to angular Fe-oxide/oxyhydroxide found in stream sediment contains minor As and Zn (Figure 4d).

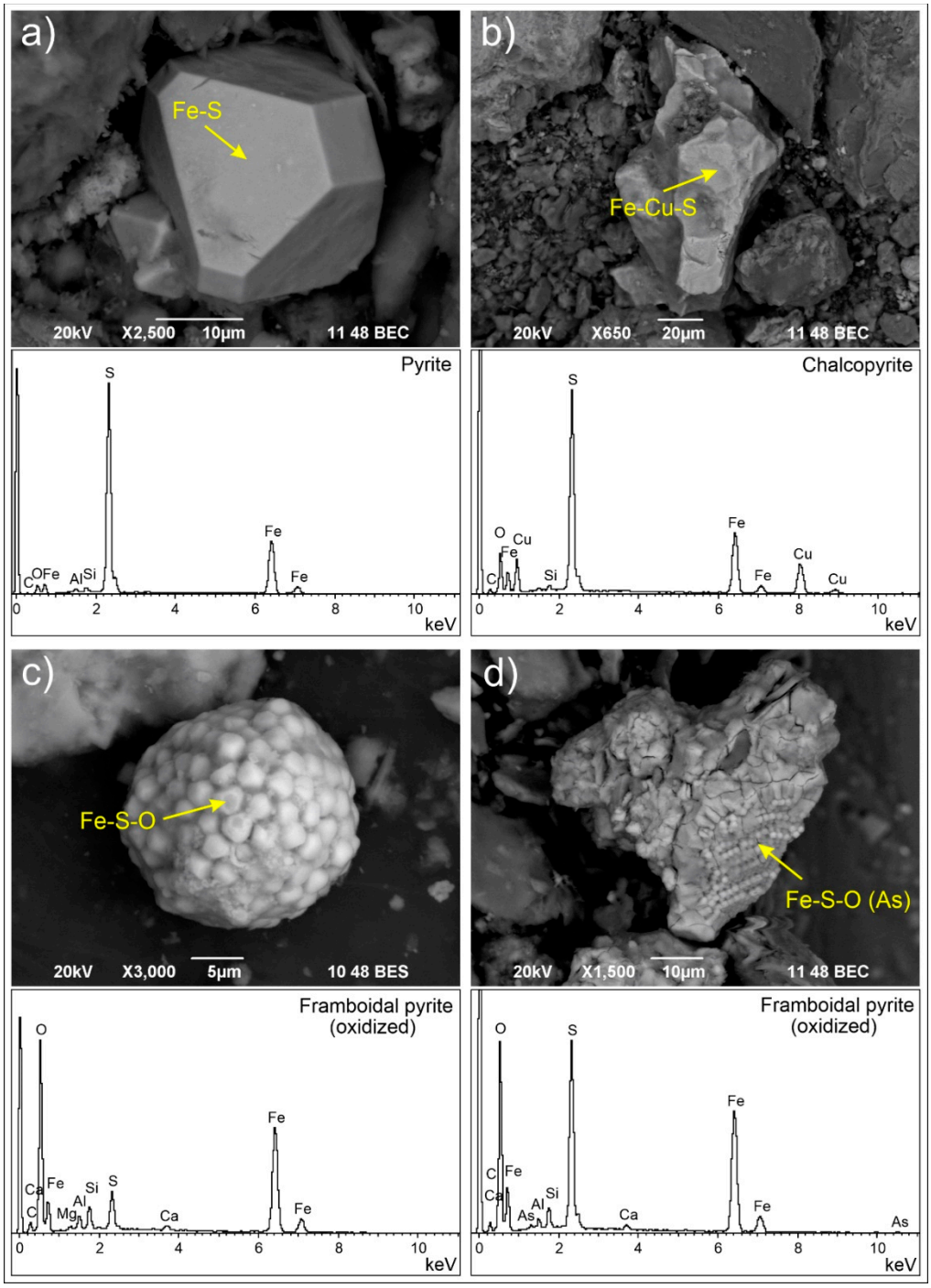

Figure 3. SEM(BSE) images and EDS spectra of solid Fe carriers in stream sediment and mine waste: (**a**) truncated pyrite octahedron; (**b**) anhedral, angular chalcopyrite; (**c**) oxidized framboidal pyrite and (**d**) oxidized framboidal pyrite with low As content showing shrinkage cracks.

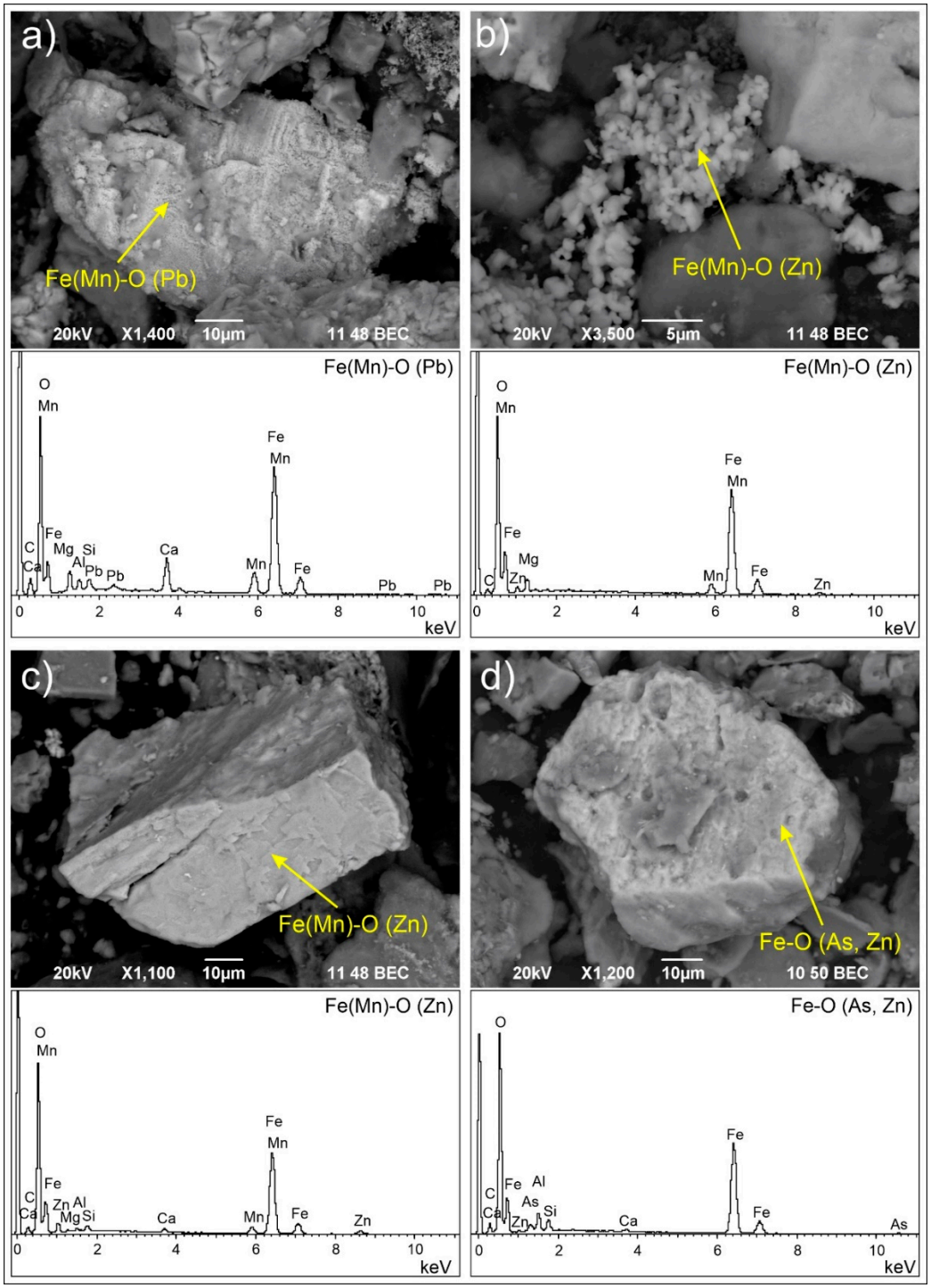

Figure 4. SEM(BSE) images and EDS spectra of solid Fe carriers in stream sediment and mine waste: (**a**) fine crystalline Fe(Mn)-oxide/oxyhydroxide coatings on an angular particle, with minor Pb content; (**b**) agglomerate of fine crystallites of Fe(Mn)-oxide/oxyhydroxide with Zn; (**c**) massive anhedral angular Fe(Mn)-O particle with minor Zn content, probably siderite; (**d**) massive anhedral subangular particle of Fe-oxide/oxyhydroxide with minor As and Zn content.

A Fe(Mn)-O phase with higher Pb content, most probably siderite, with embedded Pb-(C)-O phase, probably cerussite, was also found in the stream sediment and showed an interesting transformation of morphology. The studied particle has a perfect rhombohedral cleavage and an angular to subangular shape (Figure 5a). The part surrounding the cerussite grain has a laminated texture consisting of small platelet-shaped hexagonal

Fe(Mn)-oxide/oxyhydroxide crystals with high Pb content (Figure 5b). These platy crystals have a habit consistent with hematite [46,47]. The transformation could have occurred at the time of ore formation or in the subsequent geochemical processes following tectonic events.

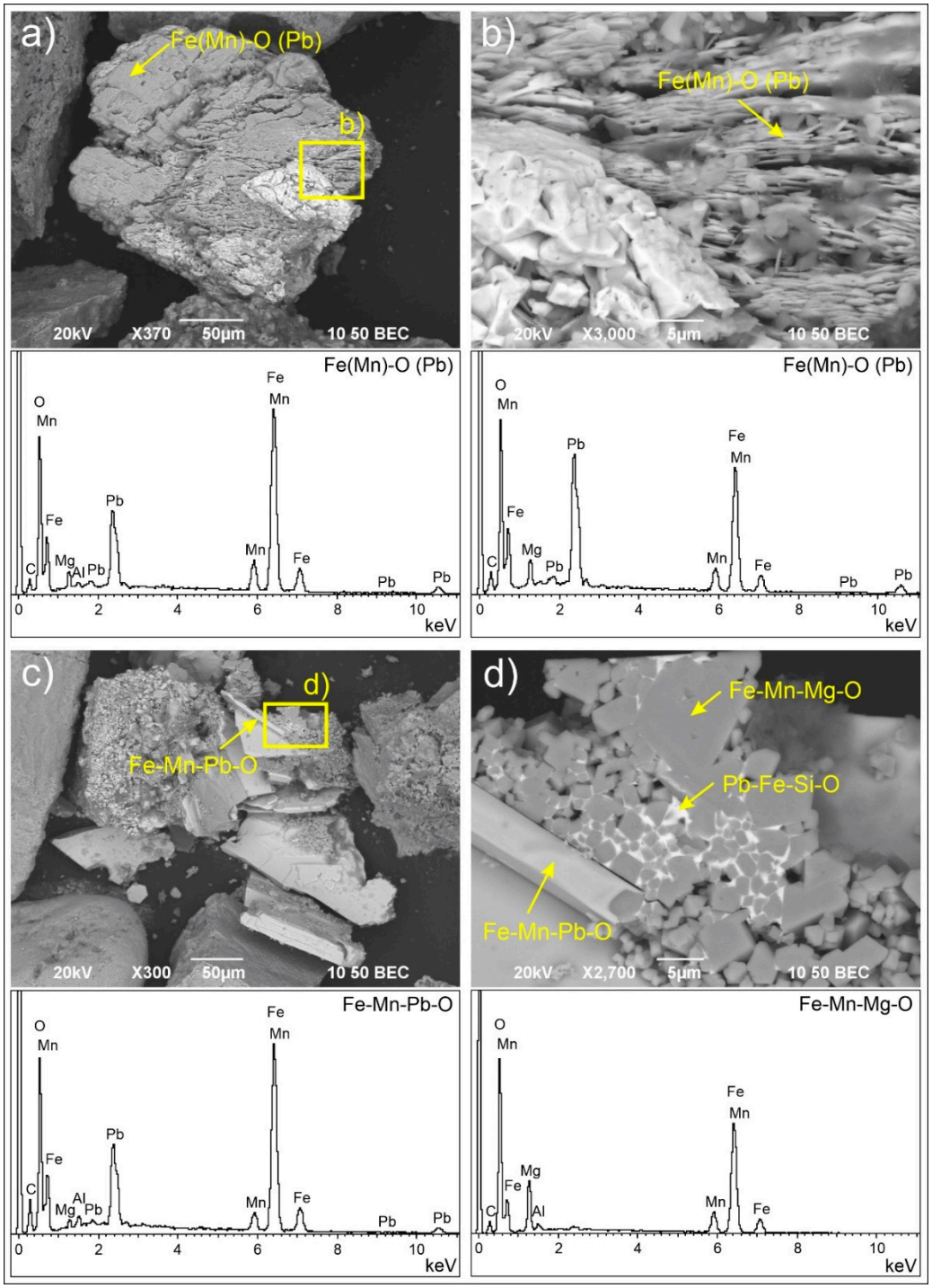

Figure 5. SEM(BSE) images and EDS spectra of solid Fe carriers in stream sediment: (**a**) large Fe(Mn)-O particle with high Pb content and embedded cerussite; (**b**) detail showing laminated hexagonal crystals of Fe(Mn)-oxides/oxyhydroxides with high Pb content; (**c**) large platy, angular Fe-Mn-Pb-oxide crystals, and (**d**) Fe-Mn-Mg-oxide with octahedral crystal habits, cemented by amorphous Pb-Fe-Si-O phase.

As an indicator of ore smelting, agglomerates of Fe-Mn-Pb-oxide (probably plumboferrite), Fe-Mn-Mg-oxide (probably jacobsite), and Pb-Fe-Si-O phase were found in the stream sediment. Agglomerates consist of large platy, angular Fe-Mn-Pb-oxide crystals (Figure 5c) and smaller Fe-Mn-Mg-oxide crystals with mostly octahedral crystal habits, which were cemented by amorphous Pb-Fe-Si-O phase (Figure 5d).

In addition to the secondary solid phases from ore processing, Fe(Mn)-oxide spherules (Figure 6a) with sizes up to 170 µm and fine Fe-O spherules with minor Cr and Ni were found in the stream sediment. The particles exhibited a dendritic surface or were composed of porous platelets, consistent with high-temperature melting and quenching in the air [48]. The large Fe(Mn)-oxide spherules probably originated from air emissions resulting from past iron ore processing, whereas the fine-sized Fe-O (Cr, Ni) spherules probably resulted from long-range atmospheric transport from steel production in Jesenice.

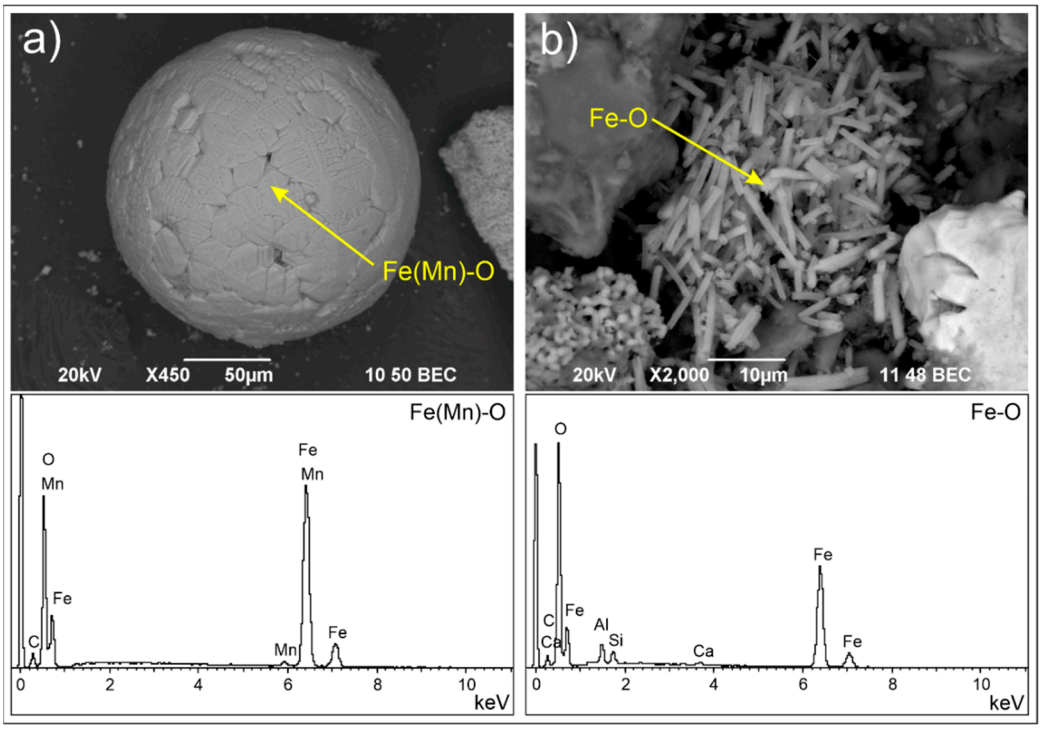

Figure 6. SEM(BSE) images and EDS spectra of solid Fe carriers in stream sediment: (**a**) Fe(Mn)-oxide spherule with a dendritic surface; (**b**) Fe-oxide/oxyhydroxide tubes.

Microtubes composed of Fe-oxide/oxyhydroxide nanoparticles (Figure 6b) were found in the stream sediment. These were probably produced by iron-oxidizing bacteria. In Hashimoto et al. [49] the sheath of microtubes was considered to be poorly crystalline Fe-oxyhydroxide, possibly 2-line ferrihydrite ($5Fe_2O_3 \cdot 9H_2O$).

In the studied stream sediments, Fe(Mn)-oxide/oxyhydroxide phases were found to be the most common sink for Pb and Zn, while Fe-oxides/oxyhydroxides also contained As and Cu.

3.2.2. Solid Zn Carriers

Sphalerite was the most abundant Zn mineral phase in stream sediments and mine waste. Sphalerite occurred in two varieties. The first was Hg-bearing sphalerite (Figure 7a), and the second was common sphalerite with various Fe contents and low Cd content (Figure 7b). Mercury-bearing sphalerite was predominantly found in stream sediments, but there were some cases also in mine waste. Mercury (Hg) content in sphalerites can be up to 5000 mg/kg [50]. According to Schroll [25], a Hg content in sphalerite of 500 mg/kg was reported for the Sava Caves. However, in the studied stream sediments, the EDS

analysis showed up to 17 wt.% Hg in sphalerite. The main characteristic of the Hg-bearing sphalerite grains was their occurrence with other Hg minerals [51], which have not been identified so far in the Sava Caves ore deposit. Both varieties were mostly anhedral, angular to subangular, and brittle fractured, due to transport abrasion. Most sphalerite particles were heavily corroded and exhibited corrosion pits, mostly along cleavage (Figure 7c) or crystal planes. These features were observed in both stream sediments and mine waste. Some sphalerite grains exhibited minor surface oxidation (Figure 7a–c). As Zn-sulphates are very soluble in water, it is unlikely that secondary sulfate solid phases would be formed [52]. The Zn-(C)-O phase, found in the stream sediment, can be described as either smithsonite, hydrozincite, or zincite, which are the secondary ore minerals or final products of sphalerite oxidative weathering (Figure 7d). The occurrence and morphology of these phases resembled those of sphalerite. The surface exhibited an uneven, pitted topography, indicating a high rate of chemical weathering of the sphalerite phase.

3.2.3. Solid Pb Carriers

Lead (Pb) ore mineral galena was less abundant as compared to sphalerite. It was mainly found dispersed in the stream sediments and in minor occurrences in mine waste. Galena occurred as euhedral to anhedral, angular particles that rarely had the cubic shape typical of galena. The particles were abraded due to the abrasion during transport and exhibited brittle fractures along the cleavage (Figure 8a). Galena mostly had oxidized surfaces. The oxidation products were usually Pb-S-O and Pb-(C)-O phases with mineral equivalents of anglesite, oxides litharge/massicot and/or cerussite. In carbonate environments, galena can be easily oxidized directly to cerussite [53], while in the studied stream sediments the galena oxidation process involved an intermediate sulfate phase. Cerussite occurred as porous particles and rarely as massive crystals or anhedral angular grains. An example of a cerussite grain with anhedral and angular morphology embedded in Fe(Mn)-oxide/oxyhydroxide was found in the stream sediment (Figure 8b). This paragenesis is consistent with ore minerals. Nevertheless, most cerussite particles appeared to be assemblages of very fine, nano-sized crystallites (Figure 8c), which is characteristic of the secondary formation. A Pb-Si-O phase was found in both crystalline and amorphous forms in stream sediments, but it was not found in mine waste. The crystalline form occurs as a cluster of bladed crystals, possibly mineral alamosite (Figure 8d). The amorphous Pb-Fe-Si-O phase occurred as cement (Figure 5d) between crystals in agglomerates of Fe-Mn-Pb oxide and Fe-Mn-Mg oxide.

Minor contents of As and Cu were detected only in the porous type of cerussite in the stream sediment. Given that galena and massive cerussite grains did not show the presence of other PTEs detectable by EDS, the subrounded Pb-(C)-O phase with As or Cu could indicate that these particles were exposed to high-temperature processes of ore processing and smelting.

3.3. Distribution of PTEs in the Environment

The contents of PTEs in the studied stream sediments and mine waste with basic statistics are presented in Table 2. The PTE contents in the stream sediments from the two geochemical background sampling locations (SJS-1 and SJS-2) were relatively similar. Their PTEs contents were relatively low compared to the Slovenian (SSM) [54] and European (ESM) [55] median values, indicating that the background area is not affected by either geogenic dispersion of ore minerals or anthropogenic activities. Minor differences in the composition of PTE in the geochemical background can be explained by the natural variability of the elements in the lithology.

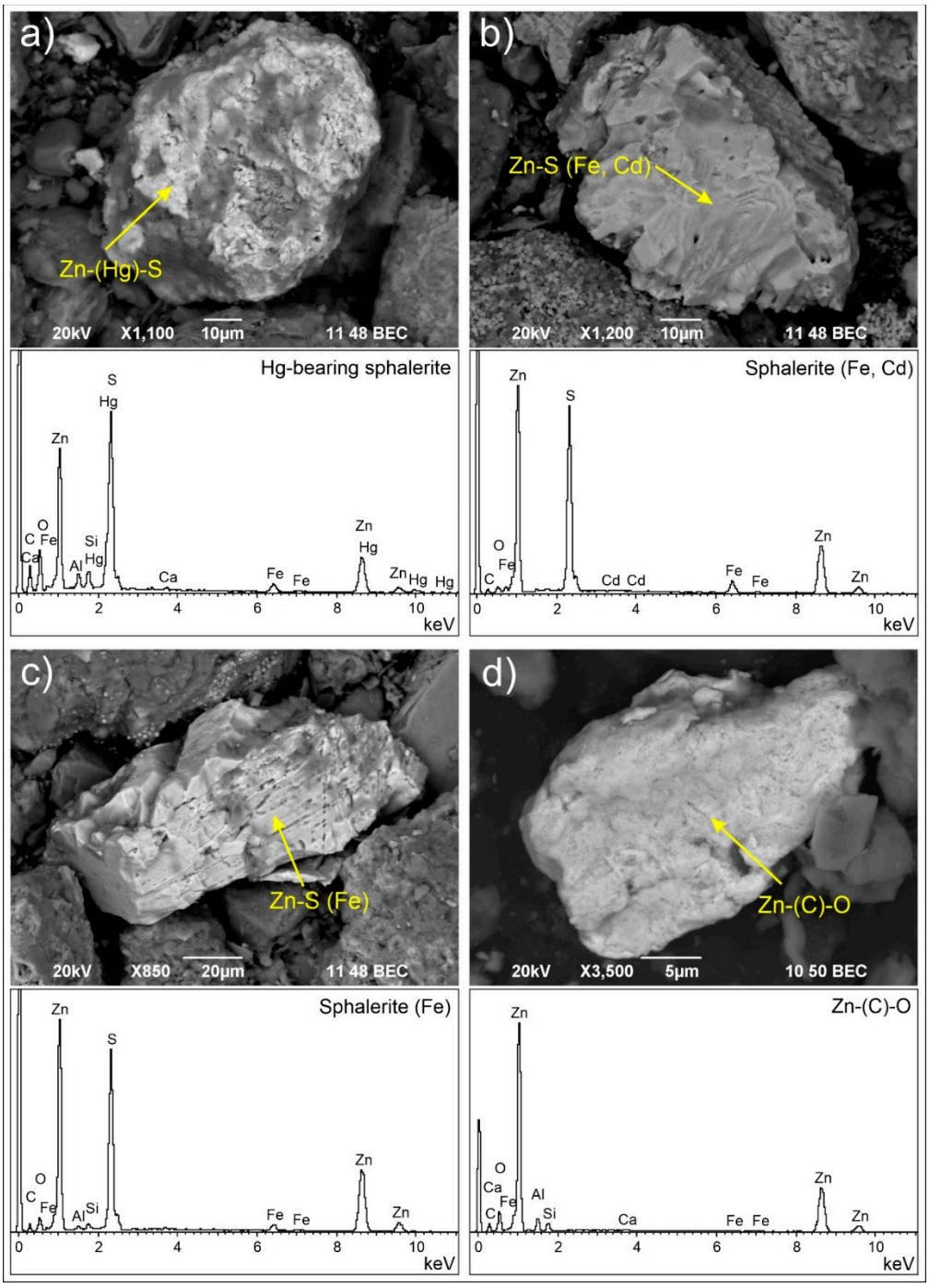

Figure 7. SEM(BSE) images and EDS spectra of solid Zn carriers in stream sediment and mine waste: (**a**) Hg-bearing sphalerite with corroded and pitted surface; (**b**) sphalerite with minor Fe and Cd; (**c**) sphalerite with minor Fe content, corroded along the cleavage; (**d**) Zn-(C)-O phase determined as either smithsonite, zincite or hydrozincite.

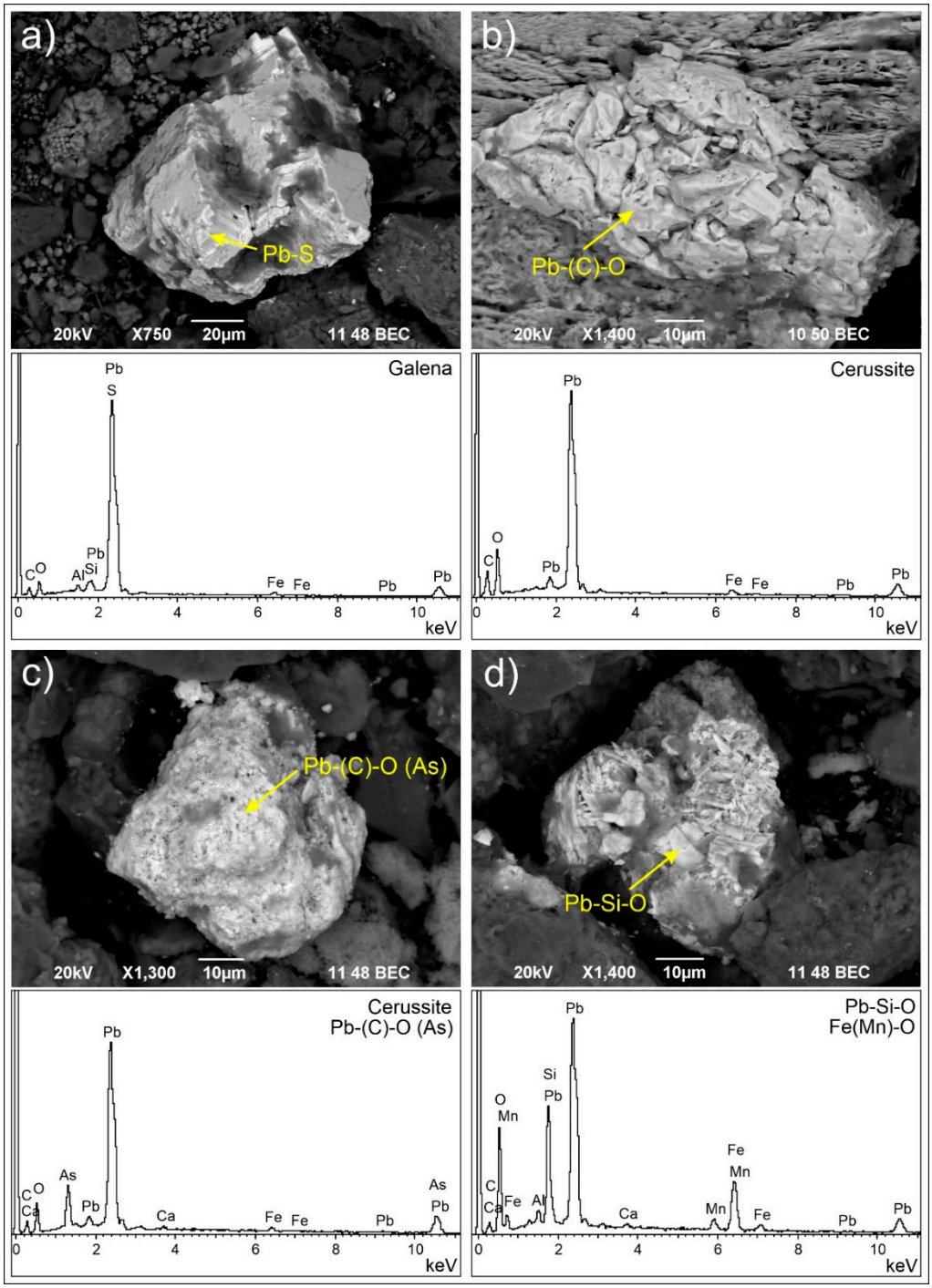

Figure 8. SEM(BSE) images and EDS spectra of solid Pb carriers in stream sediment and mine waste: (**a**) subhedral galena particle; (**b**) cerussite particle embedded in Fe(Mn)-oxide/oxyhydroxide with high Pb content; (**c**) porous Pb-(C)-O with As, probably cerussite; (**d**) cluster of Pb-Si-O crystals and Fe(Mn)-oxide/oxyhydroxide phase.

Table 2. Contents of PTEs (mg/kg), Fe (g/kg), and Mn (mg/kg) in the studied stream sediments and mine waste material. Mean, median, and standard deviation values are calculated only from samples from the mining area. Slovenian (SSM) [54] and European (ESM) [55] median values for stream sediments are shown for comparison.

Sampling Location	Sample	As	Cd	Co	Cr	Cu	Hg	Mo	Ni	Pb	Sb	Zn	Fe	Mn
Local background	**SJS-1**	7.6	1	3.9	7.8	8.4	0.1	0.80	7.9	20.1	0.4	50.8	0.9	354
	SJS-2	8.4	0.2	5	4.5	9.7	0.06	0.5	9.7	12.2	0.4	38.6	1.1	178
Mining area	**SJS-3**	38.7	0.6	16.9	14.1	34.5	2.2	0.7	34.7	35.0	0.9	170.9	3.45	713
	SJS-4	63.2	0.5	17.7	14.4	32.1	2.9	1.06	34.6	60.6	1.4	153.0	3.5	927
	SJS-5	54.8	0.6	15.3	14.1	32.2	2.9	0.96	32.5	59.2	1.3	181.7	3.5	773
	SJS-6	220.7	0.5	12.4	14.5	27.6	1.2	0.8	28.2	83.5	1.6	170.6	3.15	706
	SJS-7	91	0.8	13.6	11	27.1	2.1	0.8	29.3	82.8	1.6	221.7	3.4	718
	SJS-8	52.6	0.6	14.4	18.4	29.3	1.1	0.7	35.4	65.5	1.3	169.9	3.3	728
	SJS-9	47.1	0.6	12.2	15.4	27.2	1.4	0.6	29.9	65.2	1.2	158.9	3	575
	Mean	81.1	0.6	14.6	14.6	30.0	2.0	0.8	32.1	64.5	1.3	175.3	3.3	665
	Median	54.8	0.6	14.4	14.4	29.3	2.1	0.8	32.5	65.2	1.3	170.6	3.4	723
	St. dev.	63.7	0.1	2.1	2.2	2.9	0.8	0.2	2.9	16.4	0.2	22.5	0.2	105
Mine waste	**SJS-W**	188	2.0	22.9	26.4	56.7	8.8	3.3	77.9	153.1	11.8	253.9	4.7	1871
SSM	**Median**	7	0.4	12	66	23	0.09	-	37	22	0.4	81	3.04	695
ESM	**Median**	6	0.28	8	21	14	0.038	0.63	16	14	0.62	60	1.97	382

A relatively uniform increase in the contents of most PTEs in stream sediments was observed across the mining area. From the background area, the contents increased by at least 3 times for Co and Cr; 3 to 5 times for Ni, Pb, Sb, and Zn; 4 to 9 times for As; and as much as 36 times for Hg. The elevated contents of PTEs in the mining area are the result of both geogenic and anthropogenic influences. Cobalt (Co) and Sb were not detected in ore minerals due to the limitations of EDS analysis. However, their contents may be affected by lithological variability in the Sava Caves area and trace element contents in primary solid PTE carriers. Chromium (Cr) and Ni contents may also be affected by the anthropogenic impacts of stainless-steel production and the use of stainless steel materials. The highest Hg contents were found near the main mining outpost. A large contribution of Hg to the stream sediments was probably the dispersion of Hg-sphalerite. Galena and sphalerite are the main solid Pb and Zn carriers, along with their secondary phases. The stream sediments from the SE tributary (SJS-6) had the highest levels of As (220.7 mg/kg), which are up to 26 times higher than the background As levels. Lead (Pb) content (83.5 mg/kg) was also highest in the SE tributary (Table 2). Occurrences of realgar (α-As_4S_4) and orpiment (As_2S_3) were observed in the sandstone outcrops near this tributary. Arsenic (As) minerals may be the main contributors to the high As contents. Nevertheless, these minerals were not identified in stream sediments with SEM/EDS. Mercury (Hg) content was 1.2 mg/kg in the SE tributary. This may indicate the presence of sphalerite with a lower content of Hg in this tributary. In the next sampling location (sample SJS-7) the contents of Hg and Zn were increased in addition to As and Pb. In the vicinity of the locations of samples SJS-6 and SJS-7, the mining tunnels were once present. The deposition of mined rock near the stream probably influenced the dispersion of solid PTE carriers. Downstream from the sampling location SJS-7, stream sediments show a gradual decrease in most PTEs. Cadmium (Cd) was also found in the sphalerite in the Sava Caves, but its contents in the mining area and background were similar. This indicates a small contribution of Cd-bearing sphalerite to the content of Cd. The distribution of Fe and Mn contents, which are primarily related to the ore mineral siderite and the secondary Fe and Mn carriers, did not show major variations in the mining area. The contents were approximately three times higher than the background contents. Lithological changes from carbonate to siliciclastic rocks may also affect elevated Fe and Mn contents in the mining area.

Compared to the stream sediments, the mine waste sample showed enrichment with all PTEs, especially As, Cd, Hg, Mo, Ni, Pb, and Sb (Table 2). The elevated levels of Mo and Sb in the mine waste may indicate that they were bound to ore minerals. The Fe content

was slightly higher than in stream sediments, while the Mn content was 2.5 times higher than the mean Mo content in the stream sediments. These results confirm that mine waste contains poor ore and that historical mining had a greater impact on terrestrial than fluvial systems in the Sava Caves.

The correlation between the elements in the stream sediments was determined based on their distribution along the stream. Four groups of PTE distribution trends were determined (Figure 9a–c). In the first group (Figure 9a), As, Pb, and Sb show a similar distribution trend, indicating possible chemical associations between these three elements. Arsenic (As) deviates from the trend, since the As sulfide mineralization probably affected the composition in sample SJS-6. In the second group (Figure 9b) are Cd, Hg, and Zn, due to close associations in mineral sphalerite. Cadmium (Cd) and Zn were more gradually distributed in the mining area compared to Hg. The sampling location of sample SJS-6 appeared to be less affected by Hg, which may indicate differences in the occurrence of sphalerite. In the third group are Co, Cr, Cu, Ni, and Mo (Figure 9c). An abrupt increase from the background was followed by an almost uniform distribution. Only Mo content gradually decreased downstream of the W tributary. The distribution trends of Fe and Mn, as main constituents of the primary ore minerals and the secondary PTE carriers, are presented in Figure 9d. The comparison between the trends of elements in Group 3 and the trends of Fe and Mn shows that their distribution is closely related due to geogenic and anthropogenic associations.

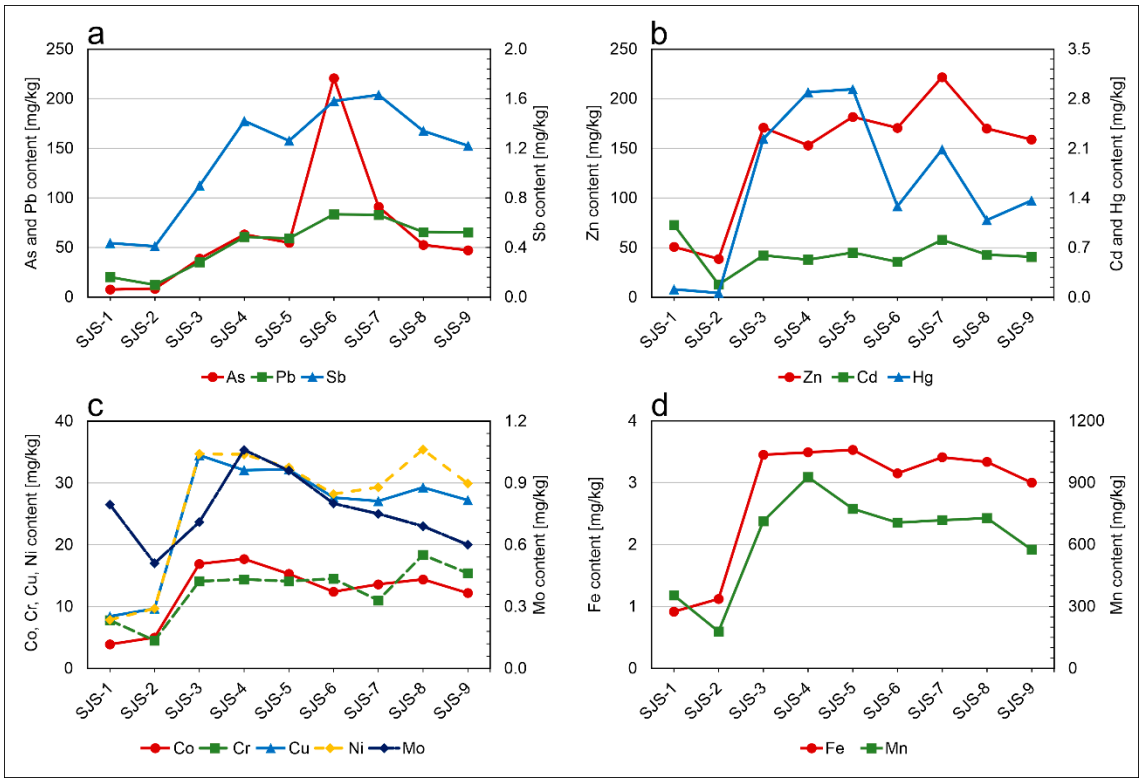

Figure 9. The distribution of PTEs according to the observed trends and correlations between PTEs: (**a**) As, Pb, and Sb; (**b**) Zn, Cd, and Hg; (**c**) Co, Cr, Cu, Ni, and Mo; and (**d**) major elements Fe and Mn.

3.4. Physico-Chemical Characteristics of Stream Water

The physico-chemical characteristics of streams normally change seasonally depending on climate (temperature, total rainfall, and rainfall intensity) and various biogeochemical processes [56]. Since stream waters in the Sava Caves were sampled only in one sampling event, the concentrations of major and trace elements provide only an insight into the current conditions of the system and its general geochemistry. The physico-chemical characteristics of the stream water are shown in Tables 3 and 4.

Table 3. Concentrations of major elements (mg/L) and physico-chemical characteristics of surface stream water–temperature (T[°C]), pH, Eh (mV), DO (mg/L), and EC (µS/cm).

Sample	Al	Ca	K	Mg	Na	S	Si	T	pH	Eh	DO	EC
SJS-1	<LOD	51.0	0.19	18.9	0.41	1	1.1	12.0	7.9	146.0	8.9	384.5
SJS-2	<LOD	46.7	0.66	15.9	0.66	2	1.7	13.9	8.5	142.0	9.0	331.6
SJS-3	0.003	58.1	0.45	18	0.60	1	1.3	11.9	8.5	122.7	9.3	371.4
SJS-4	0.009	50.6	0.66	15.5	1.1	3	1.7	13.5	8.5	129.5	9.0	331.7
SJS-5	0.004	51.5	0.62	15.3	1.44	3	1.8	12.9	8.5	127.0	9.1	359.6
SJS-6	0.003	50.4	9.8	12.1	1.46	4	2	14.9	8.0	138.1	8.4	330.8
SJS-7	0.003	52.5	3.76	15.1	1.74	4	1.9	13.0	8.5	125.2	9.1	357.0
SJS-8	0.003	51.7	1.33	15.2	1.74	4	1.9	15.0	8.5	150.3	8.9	338.4
SJS-9	0.004	42.0	5.33	13.3	1.74	4	1.9	13.7	8.5	129.1	9.2	339.3
Mean	0.0041	50.5	2.53	15.47	1.21	2.9	1.7	13.4	8.4	134.4	9.0	349.4
Median	0.003	51.0	0.66	15.30	1.44	3.0	1.8	13.5	8.5	129.5	9.0	339.3
St. dev.	0.0022	4.3	3.24	2.08	0.53	1.3	0.3	1.1	0.24	9.9	0.27	19.6

Table 4. Concentrations of PTEs (µg/L) in stream water compared. European stream water medians (ESWM) [55] are shown for comparison.

Sample	As	Cd	Co	Cr	Cu	Hg	Mo	Ni	Pb	Sb	Zn
SJS-1	0.25	0.01	0.011	<LOD	0.2	<LOD	0.2	<LOD	0.04	0.08	0.6
SJS-2	0.14	0.01	0.026	<LOD	0.3	<LOD	0.2	<LOD	0.07	0.06	0.9
SJS-3	0.24	0.01	0.011	<LOD	0.3	<LOD	0.2	<LOD	0.09	0.07	1.9
SJS-4	7.84	<LOD	0.011	<LOD	0.2	<LOD	0.2	<LOD	0.03	0.1	<LOD
SJS-5	2.36	<LOD	0.01	<LOD	0.3	<LOD	0.2	<LOD	0.03	0.11	1.3
SJS-6	2.64	0.01	0.013	<LOD	0.8	0.5	0.1	0.4	0.23	0.17	17.5
SJS-7	2.23	0.02	0.011	<LOD	0.4	<LOD	0.4	<LOD	0.15	0.16	4.3
SJS-8	1.05	<LOD	0.011	<LOD	0.5	<LOD	0.3	<LOD	0.1	0.15	7
SJS-9	0.94	<LOD	0.011	<LOD	0.4	0.3	0.3	<LOD	0.11	0.15	2.2
Mean	1.97	0.01	0.01	-	0.38	-	0.23	-	0.09	0.12	4.46
Median	1.05	0.01	0.01	-	0.30	-	0.20	-	0.09	0.11	2.05
St. dev.	2.4	0.0	0.0	-	0.2	-	0.1	-	0.1	0.04	5.7
ESWM	0.63	0.01	0.16	0.38	0.88	-	0.22	1.91	0.093	0.07	2.68

In the stream water of the Črni potok, the contents of major elements decreased in the following order: Ca > Mg > S > K > Si > Na > Al (Table 3). The geochemical characteristics of stream waters reflected the lithological characteristics of the catchment area [57]. Carbonate rocks contributed most to the chemistry of the stream waters. The slow dissolution rate of the (alumino)silicate minerals of siliciclastic lithology is also reflected in the low concentrations of Al, K, Na, and Si in the water. The downstream increase in the concentrations of K and Na corresponds to the contact of stream water with aluminosilicate minerals in shales, sandstone, and breccia. In the SE tributary, which flows over siliciclastic bedrock (sandstones and shales), the K concentration was highest. While the other major elements predominantly originated from mineral dissolution, sulfur could be released into the water via the decomposition and dissolution of organic material from soils, the atmosphere, or sulfur-bearing minerals. Under high pH conditions and in well-aerated waters, sulfur occurs mainly as a sulfate ion [58]. In general, elevated sulfate levels are expected in mining areas that promote water acidification, however total sulfur concentrations in Črni potok were extremely low compared to other areas affected by acid mine drainage [59].

The mean pH of the stream water was slightly alkaline (pH 8.4 $\pm$ 0.24) due to the dissolution of carbonates, which normally results in more basic conditions [60]. The pH and Eh (134.4 $\pm$ 9.9 mV) values indicated the slightly oxidizing conditions in the stream waters [61]. Dissolved oxygen (DO) was 9 $\pm$ 0.27 mg/L, which is typical of well-aerated streams. Because DO is temperature-dependent, a lower T value causes increased

dissolution of O_2 and vice versa [62]. The mean measured EC is in the middle range of conductivity [55] and the normal background value for most major streams. Contrary to Lacomte et al. [63], who found that in general pH, EC, and major ions increase along a stream with increasing water-rock interaction, the physico-chemical conditions were relatively uniform throughout the Črni potok creek.

The PTE concentrations in the stream water of the Črni potok are presented in Table 4. Comparison of the PTEs determined in the background stream water samples with the European stream water median values [55] showed that the concentrations of As, Co, Cu, Ni, Pb, and Zn were lower in the Črni potok, while Cd, Mo, and Sb contents were the same. The differences between the background PTE values of E and W tributary are negligible.

Mean concentrations of PTEs Co, Cu, Mo, Pb, and Sb in stream water downstream from the background area showed that the mining area probably has no major impact on water chemistry. Only As and Zn showed an increase in concentrations downstream of the background area. The highest concentrations measured were up to 40 times of mean background value for As and up to 25 times for Zn. Arsenic (As) concentrations increased in the W tributary of Črni potok in the mining area, while Zn was the highest in the SE tributary. In addition, the concentrations of Hg and Ni appeared to be higher than LOD, and a slightly higher Pb concentration was also detected in the SE tributary. This could indicate the different behavior of solid PTE carriers under the physico-chemical conditions of the SE tributary in comparison to the rest of the stream. The physico-chemical conditions of the stream water and/or mineralogical components of stream sediments appeared to support the enhanced mobility mainly of As and Zn, while other PTEs did not show significant concentrations in the stream waters.

3.5. The Behavior of Solid PTE Carriers in Stream Sediment and Interaction with Water

To understand the behavior of solid PTE carriers in stream sediments and stream waters, their mineralogical, chemical, and morphological properties were compared to physico-chemical characteristics of stream sediments and water.

All sulfide minerals found in stream sediments exhibited corrosion and oxidation features on the surfaces, which were mainly influenced by the physico-chemical conditions of the waters and probably even more by the pore waters. Given the optimum combination of DO, pH, and Eh values, the environment favored relatively rapid oxidation of Fe and As sulfides, while the transformation of Zn and Pb sulfides was probably slower [61]. Fe-sulfates, as a product of pyrite oxidation, have low stability in alkaline environments and are transformed into oxides or oxyhydroxide phases via recrystallization and secondary precipitation [41,61]. In addition, pyrite oxidation can considerably acidify waters in a mining environment [41]. However, this effect can be significantly neutralized by carbonate minerals. Arsenic (As) sulfide phases are commonly unstable in an alkaline environment, hence As becomes mobile in the aquatic environment [45,61]. Redox potential and the pH of stream waters also favor the transformation of Pb and Zn sulfides (i.e., galena and sphalerite) to oxide and/or carbonate phases [61,64]. Lead (Pb) sulfate phase (i.e., anglesite) was detected on galena surfaces, although it is soluble at pH > 6 [65] and therefore in the studied environment. Precipitation of secondary PTE-bearing carbonates in stream sediment was influenced by high pH as well as a steady influx of carbonate ions. Lead (Pb) leached from galena was, therefore, precipitated as cerussite, while the dissolution of sphalerite in stream sediments resulted in the precipitation of secondary zincite and hydrozincite rather than smithsonite. Conditions for the formation of smithsonite were probably more suitable during the alteration of the ore body since waters strongly saturated with CO_2 are favorable for the precipitation of smithsonite. These required conditions are not common for surface waters in contact with the atmosphere [64].

Fe(Mn)-oxides/oxyhydroxides and Fe-oxides/oxyhydroxides, interpreted as siderite and ferrihydrite/goethite/lepidocrocite/hematite/magnetite, are stable in alkaline environments. Both Fe and Mn-oxides/oxyhydroxides have a high affinity for certain PTEs due to the ion active sites on their surfaces [66,67]. Characteristically, these phases exhibit a

point of zero charge in a circumneutral to the alkaline environment (pH 7–10) [68], which could have influenced the concurrent removal of mobile PTEs from the stream waters of Črni potok. Lead (Pb) and Zn showed the highest binding affinity towards the Fe(Mn)-oxyhydroxide phases in stream sediments, while As was scarcely detected. The lower binding of As to these phases could be due to the alkaline conditions, since the substitution of sites occupied by As oxyanion by OH^- ions readily occurs at pH > 8 [68]. This could also explain the elevated concentrations of As in the water.

Transformations of primary ore minerals in the mine waste material were also noticeable and were similar to those in the stream sediments. Oxidized primary minerals occurred, mainly due to exposure to surface conditions, especially in contact with the atmosphere and percolating rainwater. Secondary Fe products reflected similar morphologies and chemistry to the stream sediments, but due to the surface conditions, mineralogy and degree of solid phase transformations may be different than those in the fluvial system.

4. Conclusions

The Sava Caves is an area of historical mining and ore processing, the potential environmental impacts of which were unknown to date. This study provides a comprehensive insight into the occurrence of solid PTEs carriers and their fate in the fluvial system.

The results showed that the general mineralogy of stream sediments reflected the influence of the lithology of the area. Detailed SEM/EDS analysis showed that the predominant solid PTE carriers in stream sediments and mine waste were primary ore minerals pyrite, sphalerite, galena, cerussite, chalcopyrite, and siderite. Mercury (Hg) bearing sphalerite was found as a primary solid carrier of Hg. Cadmium (Cd) was found in sphalerite, while As was found in pyrite and cerussite. Particles generally lost their primary morphological characteristics due to abrasion and corrosion during transport in the stream. The primary solid PTE carriers, particularly sulfides, tended to oxidize to secondary Fe-, Pb- and Zn-bearing minerals under slightly alkaline and oxidizing conditions in stream waters. Oxidation resulted in the formation of Fe/Mn oxide/oxyhydroxides, cerussite, anglesite, and Zn oxides/carbonates (zincite, hydrozincite, smithsonite), occurring as surface coatings or agglomerates of minute crystallites. Fe/Mn oxide/oxyhydroxides played an important role in the sequestration of PTEs, especially Pb, Zn, and partly As. The particles originating from ore processing and smelting had morphologies and chemical compositions, which are uncharacteristic of natural minerals.

The contents of most PTEs (Co, Cu, Ni, Pb, and Zn) in stream sediment were above the background levels in the mining area, but lower than in mine waste, which showed a greater impact of anthropogenic activities on the terrestrial environment. Most significant contributions were observed for As and Hg. Low concentrations of most PTEs (Cd, Co, Cu, Mo, Pb, and Sb) in stream waters indicate the stability of most secondary solid PTE carriers under current physico-chemical conditions. High As and Zn concentrations in streams indicated lower stability of solid As and Zn carriers.

This study showed that the dispersion of solid PTE carriers and thus PTEs is influenced by both geogenic and anthropogenic processes. It highlighted the importance of microchemical and micromorphological characterization of solid PTE carriers in assessing their stability in the aquatic environment. The study limitations include the lack of data on seasonal physico-chemical variability of the fluvial system, which would provide a further in-depth understanding of solid PTE carriers behavior. Future research should account for these limitations and include modeling approaches considering interactions between solid PTE carriers in stream sediments and water.

Supplementary Materials: The following supporting information can be downloaded at https://www.mdpi.com/article/10.3390/min12111424/s1: Spreadsheet S1: Chemical analysis with analytical quality control of stream sediments (SJS-1 to SJS-9) and mine waste (SJS-W); Spreadsheet S2: Chemical analysis with analytical quality control of stream waters.

Author Contributions: Conceptualization, S.K. and M.G.; methodology, S.K., M.M.; formal analysis, S.K., M.M.; investigation, S.K., M.M.; data curation, S.K.; resources, S.K., M.G., M.M.; writing—original draft preparation, S.K.; writing—review and editing, S.K., N.Z., M.G., M.M.; visualization, S.K.; supervision, N.Z., M.M.; project administration, M.M.; funding acquisition, M.M. All authors have read and agreed to the published version of the manuscript.

Funding: The authors acknowledge financial support from the state budget by the Slovenian Research Agency through the research programs Mineral Resources (P1-0025) and Groundwater and Geochemistry (P1-0020), and Palaeontology and sedimentary geology (P1-0008). The financial support was also covered from the research projects Source identification of solid pollutants in the environment on the basis of mineralogical, morphological and geochemical properties of particles (Z1-7187) and Dynamics and matter flow of potentially toxic elements (PTEs) in urban environment (J1-1713).

Data Availability Statement: Not applicable.

Conflicts of Interest: The authors declare no conflict of interest.

References

1. Adepoju, M.O.; Adekoya, J.A. Heavy metal distribution and assessment in stream sediments of River Orle, Southwestern Nigeria. *Arab. J. Geosci.* **2014**, *7*, 743–756. [CrossRef]
2. Dinelli, E.; Cortecci, G.; Lucchini, F.; Zantedeschi, E. Sources of major and trace elements in the stream sediments of the Arno River catchment (northern Tuscany, Italy). *Geochem. J.* **2005**, *33*, 531–545. [CrossRef]
3. Lim, W.Y.; Aris, A.Z.; Ismail, H.T. Spatial Geochemical Distribution and Sources of Heavy Metals in the Sediment of Langat River, Western Peninsular Malaysia. *Environ. Forensics* **2013**, *14*, 133–145. [CrossRef]
4. Calmano, W.; Hong, J.; Förstner, U. Binding and mobilization of heavy metals in contaminated sediments affected by pH and redox potential. *Water Sci. Technol.* **1993**, *28*, 223–235. [CrossRef]
5. Ashayeri, N.Y.; Keshavarzi, B. Geochemical characteristics, partitioning, quantitative source apportionment, and ecological and health risk of heavy metals in sediments and water: A case study in Shadegan Wetland, Iran. *Mar. Pollut. Bull.* **2019**, *149*, 110495. [CrossRef]
6. Miranda, L.S.; Wijesiri, B.; Ayoko, G.A.; Egodawatta, P.; Goonetilleke, A. Water-sediment interactions and mobility of heavy metals in aquatic environments. *Water Res.* **2021**, *202*, 117386. [CrossRef]
7. Krishna, A.; Mohan, K.R.K.; Murthy, N.N. A multivariate statistical approach for monitoring of heavy metals in sediments: A case study from Wailpalli Watershed, Nalgonda District, Andhra Pardesh, India. *Res. J. Environ. Earth. Sci.* **2010**, *3*, 103–113. Available online: https://maxwellsci.com/jp/abstract.php?jid=RJEES&no=89&abs=06 (accessed on 19 August 2022).
8. Budkovič, T.; Šajn, R.; Gosar, M. Environmental impact of active and abandoned mines and metal smelters in Slovenia. *Geologija* **2003**, *46*, 135–140. [CrossRef]
9. Gosar, M.; Šajn, R.; Miler, M.; Burger, A.; Bavec, Š. Overview of existing information on important closed (or in closing phase) and abandoned mining waste sites and related mines in Slovenia. *Geologija* **2020**, *63*, 221–250. [CrossRef]
10. Gosar, M.; Pirc, S.; Bidovec, M. Mercury in the Idrijca river sediments as a reflection of mining and smelting activities of the mercury mine Idrija. *J. Geochem. Explor.* **1997**, *58*, 125–131. [CrossRef]
11. Biester, H.; Gosar, M.; Covelli, S. Mercury speciation in sediments affected by dumped mining residues in the drainage area of the Idrija mercury mine, Slovenia. *Environ. Sci. Technol.* **2000**, *34*, 3330–3336. [CrossRef]
12. Gosar, M.; Šajn, R. Mercury in soil and attic dust as a reflection of Idrija mining and mineralization (Slovenia). *Geologija* **2001**, *44*, 137–159. [CrossRef]
13. Šajn, R. Factor Analysis of soil and attic-dust to separate mining and metallurgy influence, Meža valley, Slovenia. *Math. Geol.* **2006**, *38*, 735–747. [CrossRef]
14. Šajn, R.; Gosar, M. Soil pollution in surroundings of Litija as a reflection of mining, metallurgy and natural conditions. *Geologija* **2007**, *50*, 131–145. [CrossRef]
15. Šajn, R.; Gosar, M. Multivariate statistical approach to identify metal sources in Litija area (Slovenia). *J. Geochem. Explor.* **2014**, *138*, 8–21. [CrossRef]
16. Teršič, T.; Gosar, M.; Šajn, R. Impact of mining activities on soils and sediments at the historical mining area in Podljubelj, NW Slovenia. *J. Geochem. Explor.* **2009**, *1*, 1–10. [CrossRef]
17. Teršič, T.; Miler, M.; Gaberšek, M.; Gosar, M. Contents of arsenic and some other elements in stream sediments and waters of the Medija drainage basin, central Slovenia. *Geologija* **2018**, *61*, 5–35. [CrossRef]
18. Gosar, M.; Žibret, G. Mercury contents in the vertical profiles through alluvial sediments as a reflection of mining in Idrija (Slovenia). *J. Geochem. Explor.* **2011**, *110*, 81–91. [CrossRef]
19. Miler, M.; Gosar, M. Characteristics and potential environmental influences of mine waste in the area of the closed Mežica Pb-Zn mine (Slovenia). *J. Geochem. Explor.* **2012**, *112*, 152–160. [CrossRef]
20. Miler, M.; Bavec, Š.; Gosar, M. The environmental impact of historical Pb-Zn mining waste deposits in Slovenia. *J. Environ. Manag.* **2022**, *308*, 114580. [CrossRef]

21. Šorn, J. Bucelleniji in Ruardi na Savi pri Jesenicah. Ljubljana. *Kronika* **1976**, *24*, 69–74. Available online: http://www.dlib.si/?URN=URN:NBN:SI:doc-BW51LH1L (accessed on 13 September 2022).
22. Češmiga, I. *Rudarstvo LR Slovenije*; Nova Proizvodnja: Ljubljana, Slovenia, 1959.
23. Rjazancev, A. Razpad fužin in nastanek metalurške industrije na Jesenicah. *Jeklo Ljud.* **1964**, *1*, 16380162. Available online: http://www.dlib.si/?URN=URN:NBN:SI:DOC-PHHC39IL (accessed on 13 September 2022).
24. Voss, W. *Die Mineralien des Herzogthums Krain*; Kleinmayr & Fed: Bamberg, Germany, 1895; pp. 10–81.
25. Schroll, E. Ein Beitrag zur geochemischen Analyse Ostalpiner Blei-Zink Erze. *Mitt. Der Osterr. Mineral. Gesselschaft* **1954**, *3*, 41–43.
26. Slovenian Environmental Agency, Climate. Available online: https://meteo.arso.gov.si/uploads/probase/www/climate/table/sl/by_location/planina-pod-golico/climate-normals_81-10_Planina-pod-Golico.pdf (accessed on 21 October 2022).
27. Mohorič, N.; Grigillo, D.; Jemec Auflič, M.; Mikoš, M.; Celarc, B. Longitudinal profiles of torrential Channels in the Western Karavanke mountains. *Geologija* **2016**, *59*, 273–286. [CrossRef]
28. Buser, S.; Cajhen, J. *Osnovna Geološka Karta SFRJ. L 33-52, Celovec (Klagenfurt)*; [Kartografsko gradivo]. 1:100,000; Zvezni Geološki Zavod Beograd: Beograd, Serbia, 1978.
29. Iskra, M. The geologic features of the Savske jame iron ore deposit. *Geologija* **1965**, *8*, 279–298. Available online: https://www.geologija-revija.si/index.php/geologija/article/view/223 (accessed on 12 September 2022).
30. Drovenik, M.; Drovenik, F.; Pleničar, M. The origin of Slovenian ore deposits. *Geologija* **1980**, *23*, 1–157. Available online: https://www.geologija-revija.si/index.php/geologija/article/view/1743 (accessed on 13 September 2022).
31. Mikuž, V.; Vidrih, R.; Grm, M. Minerali Savskih jam in okolice. *Scopolia Suppl.* **2006**, *3*, 78–83. Available online: http://www.dlib.si/?URN=URN:NBN:SI:doc-048L4JBH (accessed on 13 September 2022).
32. De Groot, A.J.; Zschuppe, K.H.; Salomons, W. Standardization of methods of analysis for heavy metals in sediments. *Hydrobiologia* **1982**, *92*, 689–695. [CrossRef]
33. Noack, C.W.; Jain, J.C.; Stegmeier, J.; Hakala, J.A.; Karamalidis, A.K. Rare earth element geochemistry of outcrop and core samples from the Marcellus Shale. *Geochem. Trans.* **2015**, *16*, 6. [CrossRef]
34. Goldstein, J.; Newbury, D.; Joy, D. *Scanning Electron Microscopy and X-ray Microanalysis*, 3rd ed.; Kluwer Academic/Plenum Publishers: New York, NY, USA, 2003.
35. Oxford Instruments. *INCA Energy Operator Manual*; Oxford Instruments Analytical Ltd.: High Wycombe, UK, 2006.
36. Anthony, J.W.; Bideaux, R.A.; Bladh, K.W.; Nichols, M.C. *The Handbook of Mineralogy*; Mineralogical Society of America: Chantilly, VA, USA, 2009. Available online: http://www.handbookofmineralogy.org/ (accessed on 26 July 2022).
37. The Mineralogy Database. 2012. Available online: http://webmineral.com/ (accessed on 26 July 2022).
38. Reimann, C.; Demetriades, A.; Eggen, O.A.; Filzmoser, P. *EuroGeoSurveys Geochemistry Expert Group. The EuroGeoSurveys Geochemical Mapping of Agricultural and Grazing Land Soil Project (GEMAS)–Evaluation of Quality Control Results of Aqua Regia Extraction Analysis*; NGU Report 2009.049; Geological Survey of Norway: Trondheim, Norway, 2009; p. 94.
39. Oreas, OREAS 45P. Available online: https://www.oreas.com/crm/oreas-45p/ (accessed on 13 September 2022).
40. Inorganic Ventures–Products. Available online: https://www.inorganicventures.com/coa/Letterhead/IV/IV-STOCK-1643_T2-MEB720866.pdf (accessed on 13 September 2022).
41. Usher, C.R.; Cleveland, C.A.; Strongin, D.R.; Schoonen, M.A. Origin of oxygen in sulfate during pyrite oxidation with water and dissolved oxygen: An in situ horizontal attenuated total reflectance infrared spectroscopy isotope study. *Environ. Sci. Technol.* **2004**, *38*, 5604–5606. [CrossRef]
42. Huggins, F.E.; Huffman, G.P.; Kosmack, D.A.; Lowenhaupt, D.E. Mossbauer detection of goethite (α-FeOOH) in coal and its potential as an indicator of coal oxidation. *Int. J. Coal Geol.* **1980**, *1*, 75–81. [CrossRef]
43. Sileo, E.E.; Alvarez, M.; Rueda, E.H. Structural studies on the manganese for iron substitution in the synthetic goethite-jacobsite system. *Int. J. Inorg. Mater.* **2001**, *3*, 271–279. [CrossRef]
44. Rahimi, S.; Moattari, R.M.; Rajabi, L.; Derakhashan, A.A.; Keyhani, M. Iron oxide/hydroxide (α,γ-FeOOH) nanoparticles as high potential adsorbents for lead removal from polluted aquatic media. *J. Ind. Eng. Chem.* **2015**, *23*, 33–43. [CrossRef]
45. Caraballo, M.A.; Asta, M.P.; Perez, J.P.H.; Hochella, M.F. Past, present and future global influence and technological applications of iron-bearing metastable nanominerals. *Gondwana Res.* **2022**, *110*, 283–304. [CrossRef]
46. Lin, M.; Tng, L.; Lim, T.; Choo, M.; Zhang, J.; Tan, H.R.; Bai, S. Hydrothermal synthesis of octahedral hematite (α-Fe_2O_3) nanoparticles: An epitaxial growth from goethite (α-Fe_2O_3). *J. Phys. Chem.* **2014**, *118*, 10903–10910. [CrossRef]
47. Katsuki, H.; Choi, E.K.; Lee, W.J.; Hwang, K.T.; Cho, W.S.; Huang, W.; Komarneni, S. Ultrafast microwave-hydrothermal synthesis of hexagonal plates of hematite. *Mater. Chem. Phys.* **2018**, *205*, 210–216. [CrossRef]
48. Pino, M.; Abarzúa, A.M.; Astorga, G.A.; Martel-Cea, A.; Cossio-Montecinos, N.; Navarro, R.X.; Lira, M.P.; Labarca, R.; Lecompte, M.A.; Adedeji, V.; et al. Sedimentary record from Patagonia, southern Chile supports cosmic-impact triggering of biomass burning, climate change, and megafaunal extinctions at 12.8 ka. *Sci. Rep.* **2019**, *9*, 4413. [CrossRef]
49. Hashimoto, H.; Yokoyama, S.; Asaoka, H.; Kusano, Y.; Ikeda, Y.; Seno, M.; Takada, J.; Fujii, T.; Nakanishi, M.; Murakami, R. Characteristics of hollow microtubes consisting of amorphous iron oxide nanoparticles produced by iron oxidizing bacteria, *Leptothrix ochracea*. *J. Magn. Magn. Mater.* **2007**, *310*, 2405–2407. [CrossRef]
50. Schwartz, M.O. Mercury in Zinc Deposits: Economic Geology of a Polluting Element. *Inter. Geol. Rev.* **1997**, *39*, 905–923. [CrossRef]

51. Radosavljević, S.A.; Stojanović, J.N.; Pačevski, A.M. Hg-bearing sphalerite from the Rujevac polymetallic ore deposit, Podrinje metallogenic district, Serbia: Compositional variations and zoning. *Chem. Erde.* **2012**, *72*, 237–244. [CrossRef]
52. Lee, P.; Kang, M.-J.; Choi, S.-H.; Touray, J.-C. Sulfide oxidation and the natural attenuation of arsenic and trace metals in the waste rocks of the abandoned Seobo tungsten mine, Korea. *Appl. Geochem.* **2005**, *20*, 1687–1703. [CrossRef]
53. Szczerba, M.; Sawlowicz, Z. Remarks on the origin of cerussite in the Upper Silesian Zn-Pb deposits, Poland. *Mineralogia* **2009**, *40*, 53–64. [CrossRef]
54. Sotlar, K. Potočni Sediment Kot Vzorčno Sredstvo za Izdelavo Geokemične Karte Slovenije. Diploma Thesis, University of Ljubljana, Ljubljana, Slovenia, 4 December 1995.
55. Salminen, R. Part 1: Background Information, Methodology and Maps. In *Geochemical Atlas of Europe*; Salminen, R., Ed.; Geological Survey of Finland: Espoo, Finland, 2006.
56. Lintern, A.; Webb, J.A.; Ryu, D.; Liu, S.; Bende-Michl, U.; Waters, D.; Leahy, P.; Wilson, P.; Western, A.W. Key factors influencing differences in stream water quality across space. *WIREs Water* **2017**, *5*, e1260. [CrossRef]
57. Chuman, T.; Hruška, J.; Oulehle, F.; Gürtlerová, P.; Majer, V. Does stream water chemistry reflect watershed characteristics? *Environ. Monit. Assess.* **2013**, *185*, 5683–5701. [CrossRef] [PubMed]
58. Edwards, A.C.; Ferrier, R.C.; Miller, J.D. The contribution of sulphate to total sulphur in a range of natural water samples. *Hydrol. Sci. J.* **1992**, *37*, 277–283. [CrossRef]
59. Likus-Cieślik, J.; Smoliński, A.; Pietrzykowski, M.; Bąk, A. Sulphur contamination impact on seasonal and surface water chemistry on reforested area of a former sulphur mine. *Land Degrad. Dev.* **2019**, *30*, 212–225. [CrossRef]
60. Du Laing, G.; Rinklebe, J.; Vandecasteele, B.; Meers, E.; Tack, F.M. Trace metal behaviour in estuarine and riverine floodplain soils and sediments: A review. *Sci. Total. Enivron.* **2009**, *407*, 3972–3985. [CrossRef]
61. Brookins, D.G. *Eh-pH Diagrams for Geochemistry*; Springer: Berlin/Heidelberg, Germany, 1988; pp. 16–55.
62. Trick, J.K.; Stuart, M.; Reeder, S. Contaminated groundwater sampling and quality control of water analyses. In *Environmental Geochemistry*; De Vivo, B., Belkin, E.H., Lima, A., Eds.; Elsevier: Amsterdam, The Netherlands, 2008; pp. 29–57.
63. Lecomte, K.L.; García, M.G.; Formica, S.; Depetris, P.J. Influence of geomorphological variables on mountainous stream water chemistry (Sierras Pampeanas, Córdoba, Argentina). *Geomorphology* **2009**, *110*, 195–202. [CrossRef]
64. Reichert, J.; Borg, G. Numerical simulation and a geochemical model of supergene carbonate hosted non-sulphide zinc deposits. *Ore Geol. Rev.* **2008**, *33*, 134–151. [CrossRef]
65. Lin, Z. Mineralogical and chemical characterization of wastes from a sulfuric acid industry in Falun Sweden. *Environ. Geol.* **1997**, *30*, 153–162. [CrossRef]
66. Jackson, T.A.; Bistricki, T. Selective scavenging of copper, zinc, lead, and arsenic by iron and manganese oxyhydroxide coatings on plankton in lakes polluted with mine and smelter wastes: Results of energy dispersive X-ray micro-analysis. *J. Geochem. Explor.* **1995**, *52*, 97–125. [CrossRef]
67. Hou, D.; He, J.; Lu, C.; Ren, L.; Fan, Q.; Wang, J. Distribution characteristics and potential ecological risk assessment of heavy metals (Cu, Pb, Zn, Cd) in waters and sediments from Lake Dalinouer, China. *Ecotoxicol. Environ. Saf.* **2013**, *93*, 135–144. [CrossRef] [PubMed]
68. Fendorf, S.; Nico, P.; Kocar, B.D.; Masue, Y.; Tufano, K.J. *Arsenic Chemistry in Soils and Sediments*; Developments in Soil, Science; Singh, B., Gräfe, M., Eds.; Elsevier: Amsterdam, The Netherlands, 2010; Volume 34, pp. 357–378. [CrossRef]